Journal of Biomolecular NMR, **23:** 57–61, 2002.
KLUWER/ESCOM

Refinement of the solution structure of the heparin-binding domain of vascular endothelial growth factor using residual dipolar couplings

Melissa E. Stauffer[a,b,**], Nicholas J. Skelton[a] & Wayne J. Fairbrother[a,*]
[a]*Department of Protein Engineering, Genentech, Inc., 1 DNA Way, South San Francisco, CA 94080, U.S.A.;*
[b]*School of Molecular Biosciences, Washington State University, Pullman, WA 99164, U.S.A.*

Received 21 December 2001; Accepted 22 February 2002

Key words: angiogenesis, protein structure, residual dipolar couplings, vascular endothelial growth factor

Abstract

Previous NMR structural studies of the heparin-binding domain of vascular endothelial growth factor ($VEGF_{165}$) revealed a novel fold comprising two subdomains, each containing two disulfide bridges and a short two-stranded antiparallel β-sheet. The mutual orientation of the two subdomains was poorly defined by the NMR data. Heteronuclear relaxation data suggested that this disorder resulted from a relative lack of experimental restraints due to the limited size of the interface, rather than inherent high-frequency flexibility. Refinement of the structure using $^{1}H^{N}$-^{15}N residual dipolar coupling restraints results in significantly improved definition of the relative subdomain orientations.

Vascular endothelial growth factor (VEGF), an endothelial cell (EC)-specific mitogen and motogen, is a critical regulator of normal and pathological angiogenesis (Ferrara, 2001). VEGF is a covalently-linked homodimeric protein existing in at least six different isoforms resulting from alternative exon splicing. The different isoforms, containing 121, 145, 165, 183, 189, or 206 amino acids per monomer, share a common 115-residue N-terminal domain that interacts directly with the VEGF receptors Flt-1 (VEGFR-1) and KDR (VEGFR-2). The most commonly expressed isoform, $VEGF_{165}$, and longer isoforms share the same C-terminal heparin-binding domain. Removal of this heparin-binding domain from $VEGF_{165}$, either by alternative exon splicing (i.e., $VEGF_{121}$) or by plasmin cleavage, is associated with a significant loss (> 100-fold) in VEGF bioactivity (Keyt et al., 1996).

The enhanced bioactivity of the longer heparin-binding isoforms of VEGF has been attributed recently to the formation of ternary VEGF/KDR/neuropilin-1 complexes (Whitaker et al., 2001). Neuropilin-1 (NP-1) was identified previously as an isoform-specific VEGF receptor that binds $VEGF_{165}$ but not $VEGF_{121}$; the VEGF heparin-binding domain was identified as the epitope for NP-1 binding (Soker et al., 1998). When cotransfected into KDR-expressing cells, NP-1 enhances the binding of $VEGF_{165}$ to KDR and increases the KDR-mediated mitogenic and chemotactic activity of VEGF (Soker et al., 1998). More recently, *in vitro* experiments have established that the VEGF heparin-binding domain-mediated interaction with NP-1 increases the affinity of $VEGF_{165}$ for KDR (Fuh et al., 2000). Furthermore, the affinity of $VEGF_{165}$ for the NP-1 extracellular domain is greatly enhanced by the addition of heparin (Fuh et al., 2000). Blocking $VEGF_{165}$ binding to NP-1 with GST-fused VEGF heparin-binding domain inhibits its binding to KDR and its EC-mitogenic activity (Soker et al., 1997, 1998). Interestingly, NP-1 is also expressed by tumor cells, where it acts as a positive modulator of angiogenesis (Soker et al., 1998; Miao et al., 2000); overexpression of a soluble variant of NP-1, that inhibits $VEGF_{165}$ binding to cell-bound NP-1, leads to tumors with extensive hemorrhage, damaged blood vessels, and apoptotic tumor cells (Gagnon et al., 2000). Antagonists of the VEGF heparin-binding domain/NP-1

*To whom correspondence should be addressed. E-mail: fairbro@gene.com
**Present address: Department of Biochemistry, Vanderbilt University, Nashville, TN 37232, U.S.A.

interaction may therefore be useful for the treatment of cancer.

We have reported previously the solution structure of the 55-residue C-terminal heparin-binding domain of $VEGF_{165}$ (hereafter referred to as $VEGF_{55}$) (Fairbrother et al., 1998). The novel heparin-binding domain fold comprises two sub-domains, each containing a small two-stranded anti-parallel β-sheet and two disulfide bonds; the C-terminal subdomain also contains a short α-helix that packs against the β-sheet. The orientation of the two subdomains with respect to each other is poorly defined. ^{15}N-relaxation data indicate that the lack of definition results from a lack of experimental restraints, due to the limited size of the subdomain interface, rather than inherent flexibility on the picosecond time scale. We report here refinement of the structure of $VEGF_{55}$ using $^{1}H^{N}$-^{15}N residual dipolar coupling (RDC) data (Tjandra and Bax, 1997), resulting in significantly improved definition of the relative subdomain orientations.

Spectra were acquired at 27 °C on a Bruker DRX-500 spectrometer equipped with a 5-mm inverse triple-resonance probe with three-axis gradient coils, unless stated otherwise. A broad-band inverse probehead was used for acquiring ^{31}P spectra. Spectra were processed and analyzed using FELIX (Molecular Simulations, Inc.).

The ^{15}N-labeled sample of $VEGF_{55}$ used for the original structure determination (Fairbrother et al., 1998) was used also in the present work. The isotropic NMR sample contained 2.0 mM protein in 25 mM sodium d_3-acetate (pH 5.5), 50 mM NaCl, 0.02% NaN_3, 10% D_2O. Partial alignment was achieved by diluting the isotropic sample (3.5-fold) into a liquid-crystalline bicelle medium comprising a mixture (4.0:1.0:0.2) of ditridecanoyl-phosphatidylcholine (DTPC), dihexanoyl-phosphatidylcholine (DHPC), and cetyltrimethylammonium bromide (CTAB) in the same buffer, to give 5% w/v total lipid (Ottiger and Bax, 1998; Losonczi and Prestegard, 1998). Based on ^{2}H quadrupole splittings and ^{31}P spectra the liquid-crystalline phase of this mixture is stable between 25–35 °C.

$^{1}H^{N}$-^{15}N splittings were measured under isotropic and partially aligned conditions using 2D IPAP ^{1}H-^{15}N HSQC experiments (Ottiger et al., 1998). Residual $^{1}D_{NH}$ dipolar couplings were extracted by subtracting the $^{1}J_{NH}$ scalar coupling constant, measured using the isotropic sample, from the $^{1}J_{NH} + {}^{1}D_{NH}$ values obtained using the liquid-crystalline bicelle sample (Figure 1). Significant broadening observed

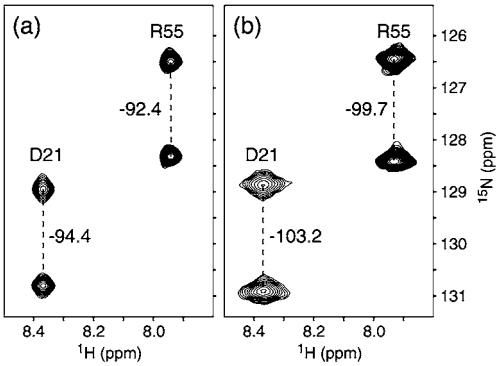

Figure 1. Superposition of selected sections from the 2D IPAP ^{1}H-^{15}N HSQC spectra of the (a) isotropic and (b) partially aligned samples of $VEGF_{55}$.

for some amide resonances suggests that the highly basic $VEGF_{55}$ interacts to some extent with the lipid bicelles. Lack of significant chemical shift changes indicates, however, that such interactions do not perturb the solution conformation of the protein. In cases where the faster relaxing upfield component of the IPAP ^{1}H-^{15}N HSQC was too broad for accurate measurement, $^{1}J_{NH} + {}^{1}D_{NH}$ was determined by comparison of the slower relaxing downfield component with a regular decoupled ^{1}H-^{15}N HSQC spectrum acquired using the same sample. Uncertainties in $^{1}D_{NH}$ were estimated to be 1, 2 or 4 Hz depending on the degree of line broadening. The residual $^{1}D_{NH}$ dipolar couplings and uncertainties measured for $VEGF_{55}$ are summarized in Figure 2a.

The residual dipolar coupling between two nuclei is given by:

$$D(\theta,\phi) = D_a\left\{(3\cos^2\theta - 1) + \tfrac{3}{2}R(\sin^2\theta\,\cos 2\phi)\right\}, \quad (1)$$

where R is the rhombicity defined as D_r/D_a; D_a and D_r are the axial and rhombic components of the alignment tensor given by $\frac{1}{3}[D_{zz} - (D_{xx} + D_{yy})/2]$ and $\frac{1}{3}[D_{xx} - D_{yy}]$, respectively; and θ and φ are the cylindrical coordinates describing the orientation of the internuclear vector in the principal axis system of the molecular alignment tensor (Tjandra and Bax, 1997). The values of D_a and R were estimated to be 16.0 ± 0.5 Hz and 0.27 ± 0.04, respectively, by fitting the experimental RDC values for 18 residues in the well-defined C-terminal subdomain of $VEGF_{55}$ to the original ensemble of 20 structures (PDB accession code 1VGH) using a simple Powell optimization

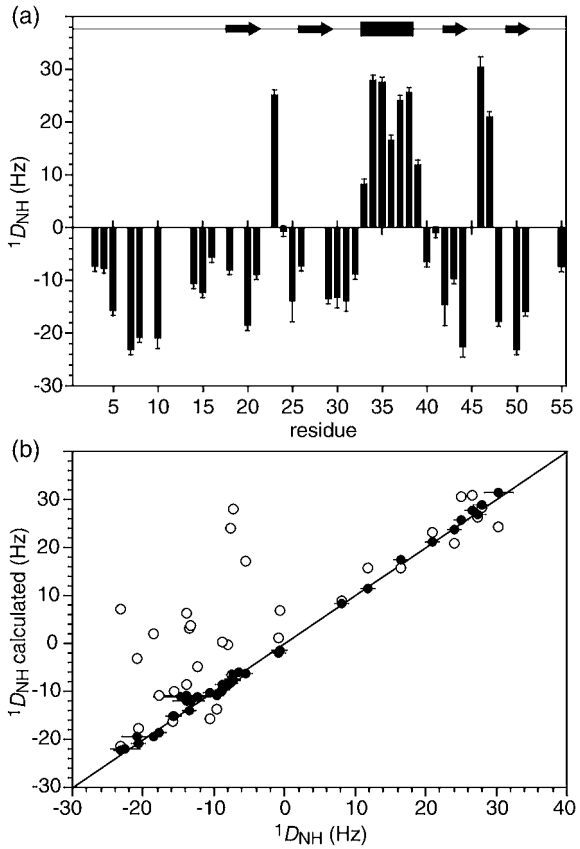

Figure 2. (a) Plot of $^1D_{NH}$ versus residue number for $VEGF_{55}$. The secondary structure of the domain is indicated. (b) Correlation between observed and calculated $^1D_{NH}$ for refinements with (filled) and without (open) RDC restraints. The structure refined with RDC restraints corresponds to that with the lowest total restraint violation energy; values of D_a and R determined for this fit are 16.3 Hz and 0.25, respectively. For the structure refined without RDC restraints the magnitude and orientation of the alignment tensor were optimized using RDC data for 18 residues in the well-defined C-terminal subdomain only (attempts to fit all the RDC data failed to converge). Values of D_a and R determined for this fit are 15.7 Hz and 0.29, respectively.

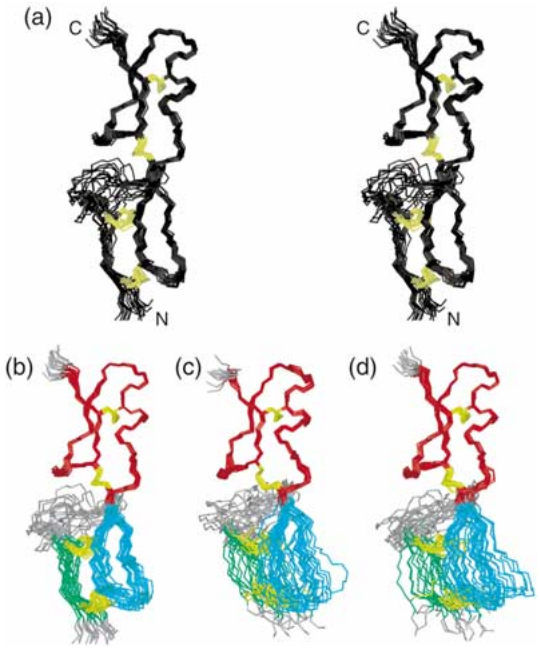

Figure 3. (a) Stereoview showing the best fit superposition, optimized using the ordered residues 7–10 and 18–52, of the 20 RDC-refined structures of $VEGF_{55}$. The backbone atoms of residues 6–53 and the sidechain heavy atoms of the 8 Cys residues are shown. Superposition on the backbone atoms of residues 29–52 (red) for the (b) CNX (with RDC restraints), (c) original (PDB accession code 1VGH), and (d) CNX (without RDC restraints) ensembles illustrates the improved definition in the relative orientation of the two subdomains afforded by RDC-refinement. In the N-terminal subdomains residues 7–10 and 18–28 are colored green and cyan, respectively.

procedure (Tjandra and Bax, 1997). Similar values (16.2 ± 0.2 Hz and 0.25 ± 0.01, respectively) were obtained by order matrix analysis of the experimental RDC values using singular value decomposition (Losonczi et al., 1999).

Structures were calculated by simulated annealing in torsion angle space (Stein et al., 1997), starting from the previously reported structure, followed by conventional simulated annealing in cartesian space (Nilges et al., 1988), using the program CNX (Molecular Simulations, Inc.). The target function included a square-well pseudo-potential for RDC restraints in which E_{RDC} is evaluated by calculating the angles θ and ϕ between the N–H bond vectors and an external axis system (Clore et al., 1998). The force constant for the RDC energy was increased from 0.001 to 1 kcal mol^{-1} Hz^{-2}, together with the force constant for the NOE-distance restraint energy, during the cooling stage. The NOE-derived distance, hydrogen-bond, and dihedral angle restraints used were identical to those used previously (Fairbrother et al., 1998). The 20 structures with the lowest residual restraint violation energies were selected to represent the RDC-refined structure of $VEGF_{55}$ (Figure 3a). Structural statistics are summarized in Table 1, together with statistics from the original NMR structure determination, that was carried out without RDC restraints using a hybrid distance geometry-simulated annealing approach followed by restrained molecular dynamics using the program DISCOVER and the AMBER forcefield (Fairbrother et al., 1998). To determine the effect of including RDC restraints in the CNX-based structure refinement a family of structures was refined

Table 1. Summary of structural statistics

	CNX refinement (with RDC)	Original NMR refinement	CNX refinement (without RDC)
RMSD from restraints			
NOE distance (Å)	0.005 ± 0.001	0.008 ± 0.002	0.005 ± 0.001
H-bond (Å)	0.007 ± 0.003	0.001 ± 0.001	0.008 ± 0.003
Dihedral angle (°)	0.18 ± 0.07	0.30 ± 0.06	0.17 ± 0.05
RDC (Hz)	1.00 ± 0.08	–	–
NOE-distance violations			
Number > 0.1 Å	0	0.6 ± 0.7	0
Max. violation (Å)	0.06 ± 0.02	0.1 ± 0.05	0.06 ± 0.02
Dihedral angle violations			
Number > 1°	0.7 ± 0.7	1.6 ± 1.0	0.3 ± 0.6
Max. violation (°)	1.1 ± 0.4	1.4 ± 0.3	0.9 ± 0.4
RMSD from idealized geometry			
Bonds (Å)	0.0031 ± 0.0003	0.0048 ± 0.0001	0.0022 ± 0.0002
Angles (°)	0.47 ± 0.03	1.57 ± 0.04	0.39 ± 0.02
Impropers (°)	0.26 ± 0.04	2.30 ± 0.14	0.14 ± 0.01
Ramachandran statistics for ordered residues[a]			
Most favored	85.0%	88.1%	83.0%
Additionally allowed	14.7%	11.9%	16.8%
Generously allowed	0.3%	0.0%	0.3%
Backbone RMSD from mean (Å)			
7–10, 18–52	0.51 ± 0.10	0.76 ± 0.19	0.79 ± 0.18
7–10, 18–29	0.42 ± 0.06	0.59 ± 0.11	0.55 ± 0.10
18–52	0.40 ± 0.07	0.60 ± 0.19	0.63 ± 0.18
18–29	0.22 ± 0.05	0.32 ± 0.07	0.29 ± 0.08
29–52	0.27 ± 0.06	0.26 ± 0.05	0.36 ± 0.09

[a]Ramachandran statistics were determined for residues 7–10 and 17–52 using PROCHECK_NMR (Laskowski et al., 1996).

using the same protocol but without RDC restraints (Table 1).

As observed for the original NMR refinement, several regions of $VEGF_{55}$ remain poorly ordered in the RDC-refined structure, including the N- and C-terminal regions (residues 1–6 and 53–55) and the loop comprising residues 11–17 (Figure 3a). Reduced ^{1}H–^{15}N NOEs for residues 2–5, Arg13 and Arg55 indicate that these regions are significantly more flexible than the remainder of the protein (Fairbrother et al., 1998). The secondary structure and subdomain architecture are also identical to the structure refined without RDC restraints.

The RDC-refined structures agree considerably better with the experimental RDC data than the structures refined without RDC restraints (Figure 2b). The improved fit to the experimental RDC restraints is associated with an improvement in the overall precision of the structural ensemble; superposition of the backbone atoms (N, C^{α}, C') of the ordered residues, 7–10 and 18–52, yields average atomic RMS deviations with respect to the mean coordinates of 0.51 Å for the RDC-refined structures and 0.76 and 0.79 Å for the structures refined without RDC restraints (Table 1; Figure 3). The improvement in the overall precision of the structure ensemble results from both improved precision in definition of the N-terminal subdomain (Table 1), and most notably, improved definition in the relative orientation of the two subdomains (Figure 3). The precision of the C-terminal subdomain is not affected significantly by inclusion of the RDC restraints, suggesting that the structure of this sub-

domain is already well defined by the short-range NOE-derived distance and dihedral angle restraints. Comparison of the CNX-refined structures indicates that the agreement with the NOE-derived distance and dihedral angle restraints is also not affected by incorporation of the RDC restraints (i.e. these restraints are equally well satisfied by both structures). Improvements relative to the original DISCOVER-based refinement likely represent differences in the forcefields used.

In summary, we have used residual dipolar couplings to refine the structure of the VEGF heparin-binding domain. The long-range geometric information contained in the RDC restraints allows for significantly more precise definition of the relative orientations of the two subdomains of this protein. Such precision is not attainable for this structure using only NOE-derived distance and dihedral angle restraints, due mainly to the qualitative and short-range nature of these restraints, together with the small size of the subdomain interface.

The RDC-refined structure has been submitted to the PDB (accession code 1KMX). Chemical shift assignments have been deposited with the BioMagResBank (accession No. 5238).

Acknowledgements

We thank G. Fuh and M. Starovasnik for discussions and assistance, M. Champe for ^{15}N-labeled VEGF heparin-binding domain, and A. Bax, J. Losonczi, J. Prestegard, and N. Tjandra for advice and software.

References

Clore, G.M., Gronenborn, A.M. and Tjandra, N. (1998) *J. Magn. Reson.*, **131**, 159–162.

Fairbrother, W.J., Champe, M.A., Christinger, H.W., Keyt, B.A. and Starovasnik, M.A. (1998) *Structure*, **6**, 637–648.

Ferrara, N. (2001) *Am. J. Physiol. Cell Physiol.*, **280**, C1358–C1366.

Fuh, G., Garcia, K.C. and de Vos, A.M. (2000) *J. Biol. Chem.*, **275**, 26690–26695.

Gagnon, M.L., Bielenberg, D.R., Gechtman, Z., Miao, H.-Q., Takashima, S., Soker, S. and Klagsbrun, M. (2000) *Proc. Natl. Acad. Sci. USA*, **97**, 2573–2578.

Keyt, B.A., Berleau, L.T., Nguyen, H.V., Chen, H., Heinsohn, H., Vandlen, R. and Ferrara, N. (1996) *J. Biol. Chem.*, **271**, 7788–7795.

Laskowski, R.A., Rullman, J.A.C., MacArthur, M.W., Kaptein, R. and Thornton, J.M. (1996) *J. Biomol. NMR*, **8**, 477–486.

Losonczi, J.A. and Prestegard, J.H. (1998) *J. Biomol. NMR*, **12**, 447–451.

Losonczi, J.A., Andrec, M., Fischer, M.W.F. and Prestegard, J.H. (1999) *J. Magn. Reson.*, **138**, 334–342.

Miao, H.-Q., Lee, P., Lin, H., Soker, S. and Klagsbrun, M. (2000) *Faseb. J.*, **14**, 2532–2539.

Nilges, M., Clore, G.M. and Gronenborn, A.M. (1988) *FEBS Lett.*, **239**, 317–324.

Ottiger, M. and Bax, A. (1998) *J. Biomol. NMR*, **12**, 361–372.

Ottiger, M., Delaglio, F. and Bax, A. (1998) *J. Magn. Reson.*, **131**, 373–378.

Soker, S., Gollamudi-Payne, S., Fidder, H., Charmahelli, H. and Klagsbrun, M. (1997) *J. Biol. Chem.*, **272**, 31582–31588.

Soker, S., Takashima, S., Miao, H.Q., Neufeld, G. and Klagsbrun, M. (1998) *Cell*, **92**, 735–745.

Stein, E.G., Rice, L.M. and Brünger, A.T. (1997) *J. Magn. Reson.*, **124**, 154–164.

Tjandra, N. and Bax, A. (1997) *Science*, **278**, 1111–1114.

Whitaker, G.B., Limberg, B.J. and Rosenbaum, J.S. (2001) *J. Biol. Chem.*, **276**, 25520–25531.